Arctic Science

OPEN ACCESS | Article

# Factors affecting river turbidity in a degrading permafrost environment: the Tasiapik River, Umiujaq (Nunavik)

**Frédéric Manseau[a], Najat Bhiry[a], John Molson[b], and Danielle Cloutier[c]**

[a]Department of Geography and Centre d'études nordiques, Université Laval, Québec, QC G1V 0A6, Canada; [b]Department of Geology and Geological Engineering and Centre d'études nordiques, Université Laval, Québec, QC G1V 0A6, Canada; [c]Department of Geography, Faculté de foresterie, de géographie et de géomatique, Université Laval, Québec, QC G1V 0A6, Canada

Corresponding author: **Najat Bhiry** (email: najat.bhiry@cen.ulaval.ca)



## Abstract

This study focuses on spatiotemporal changes in water turbidity in relation to permafrost to document the impact of meteorological conditions and water flow on hydro-sedimentary processes in northern regions. Starting in June of 2019, water turbidity data were collected at six sites along the Tasiapik River (Nunavik). A statistical analysis was completed based on records of water turbidity, precipitation, water flow, and air temperature. Our results show a significant correlation between air temperatures and turbidity, with a correlation of up to $r = 0.59$. These correlations depend on the location of the site along the river and the time of the study period (June–October 2019). The flow rate was the primary factor that caused variations in the turbidity of the Tasiapik River. Our results showed that following an increase in flow rate, there was an almost simultaneous increase in turbidity due to erosion of the banks. The duration and intensity of precipitation events are also important factors affecting the process of sediment transport. Even though meteorological conditions play an important role in turbidity variation, other characteristics of the site such as the topography and the existence of thermokarst lakes are additional factors that influence the dynamics of sediment transport in the Tasiapik River.

**Key words:** river turbidity, meteorological conditions, Nunavik, permafrost degradation

## Résumé

Les travaux menés en Arctique et Subarctique démontrent une accélération de la dégradation du pergélisol durant les dernières décennies, provoquant des tassements importants du sol et par le fait même, un accroissement du fluage d'eau chargée de sédiments vers les lacs et les rivières. Cette étude vise à mieux comprendre la variation spatio-temporelle de la turbidité fluviale en contexte périglaciaire dans le but de faire avancer les connaissances sur les impacts des conditions météorologiques et du débit sur les processus hydrosédimentaires des régions nordiques. Des données de turbidité de l'eau de la rivière Tasiapik, située à 5 km à l'est du village d'Umiujaq (Nunavik), ont été enregistrées de juin à octobre 2019 dans six sites distincts. Des analyses statistiques réalisées sur ces enregistrements indiquent qu'il existe une corrélation significative ($r = 0{,}59$) entre les températures de l'air et la turbidité de la rivière. Ces relations sont plus ou moins importantes selon l'emplacement du site le long de la rivière et selon le moment de la période d'étude. Le débit était le principal facteur à l'origine des variations de la turbidité de la rivière Tasiapik. Nos résultats ont montré qu'à la suite d'une augmentation du débit, il y a eu une augmentation presque simultanée de la turbidité due à l'érosion des berges et de la quantité des sédiments en suspension. La durée et l'intensité des précipitations sont également des facteurs importants ayant fait varier la turbidité de la rivière. Bien que les conditions météorologiques jouent un rôle important dans la variation de la turbidité, il s'est avéré que les caractéristiques du site telles que la topographie et la présence de lacs thermokarstiques sont des facteurs importants dans la dynamique du transport sédimentaire de la rivière Tasiapik. [Traduit par la Rédaction]

**Mots-clés :** turbidité des rivières, conditions météorologiques, Nunavik, dégradation du pergélisol

## Introduction

The consequences of global warming due to climate change are occurring at a much faster rate in arctic and subarctic environments (IPCC 2014; Brown et al. 2012; Ouranos 2015). One of the main concerns of global warming in these environments is the rapid degradation of permafrost (e.g., Haeberli and Hohmann 2008; Beck et al. 2015; Ran et al. 2018; Holloway and Lewkowicz 2020), which negatively af-

fects communities, ecosystems, geosystems, and the hydrosphere.

The impact of permafrost degradation on the hydrosphere occurs in various ways, but it is especially acute on river baseflow and groundwater flow systems. For example, permafrost degradation can affect groundwater flow and groundwater recharge (Bense et al. 2009; McKenzie and Voss 2013; Walvoord and Kurylyk 2016; Cochand et al. 2019; 2020). With regard to surface water, permafrost degradation may trigger an increase in a river's total suspended sediments, known as turbidity (Syvitski 2002). This sediment increase is mainly due to an increase in mass movement processes on the river banks, where abnormally high air temperatures cause rapid deepening of the active layer, which generates mass movement (Lewis et al. 2005; Lewkowicz and Harris 2005; Lamoureux and Lafrenière 2009; Jolivel and Allard 2017).

Another cause of increasing sediment transport in lakes and rivers is associated with thermokarst processes: the collapse of palsas (frost mounds covered by peat) and lithalsas (frost mineral mounds) in the permafrost environment leads to the formation of thermokarst lakes. These lakes serve as basins for meltwater and runoff, which causes them to be filled with sediments. The lakes also contribute to the thermal degradation of permafrost (Seguin and Allard 1984).

The causes of surface water turbidity variations have been examined in several studies in many regions of the world. Nevertheless, very few studies have focused on the link between turbidity and permafrost degradation (e.g., Favaro and Lamoureux 2015; Vonk et al. 2015; Jolivel and Allard 2017). High levels of turbidity in rivers and lakes have been associated with multiple environmental issues: for example, it is partly responsible for the decline in the predation success rate of certain fish species (Minello and Benfield 2018) and for the alteration of the structure of fish gills (Cumming and Herbert 2016). There is a greater need to monitor surface water turbidity in northern communities that are more dependent on these water sources. In Nunavik (Quebec, Canada), the drinking water for 12 of the 14 communities comes from surface water. It is therefore important to document the quality of the aquatic ecosystems in these regions, including water quality and turbidity, to ensure, among other things, the sustainability and accessibility of drinking water.

The main objective of this study was to better understand the spatio-temporal variation of fluvial turbidity in a periglacial context to document the impact of climate change on hydro-sedimentary processes in northern regions.

## Study area

This research was conducted in the Tasiapik Valley (Fig. 1), a small watershed located 5 km east of the village of Umiujaq (56°33′ N, 76°31′ W) on the eastern coast of Hudson Bay (Quebec, Canada). The watershed is bordered to the northeast by Umiujaq Hill and to the southwest by the cuesta cliffs, the distal parts of which were formed from talus and cones. Snow avalanches have been identified as an important process for debris remobilization on the talus slopes (Veilleux et al. 2020). The valley is drained by a main stream and its tributaries, which flow approximately 4.5 km southward to Lake Tasiujaq, a brackish 691 km$^2$ lake connected to Hudson Bay. The width of the stream varies between 0.5 m at its upstream part and 75 m at the mouth; the depth rarely exceeds 1 m. According to Lemieux et al. (2020), the stream is mostly supplied by surface drainage during the summer, but groundwater also flows upward to the stream, especially during the winter. As this stream does not have an official name, we refer to it as the Tasiapik River in this paper.

The Umiujaq region is located in the Superior geological province, consisting of igneous and metamorphic rocks dating from the Neoarchean (−2.73 and −2.68 Ga) (Chandler 1988; Eaton and Darbyshire 2010). The western part of the valley is composed of a sequence of volcano-sedimentary rock dating from the Paleoproterozoic (Chandler 1988; Eaton and Darbyshire 2010; Lemieux et al. 2016). This sequence creates an asymmetric monoclinal relief form called a cuesta, which is formed by a steep front oriented to the east and a more gradual slope in the back leading to the west toward Hudson Bay. A sequence of Quaternary deposits was established during the retreat of the Laurentide ice sheet, which began at around 8200 BP (Lavoie et al. 2012). According to Banville (2016), Fortier et al. (2020), and Lemieux et al. (2020), the Quaternary deposits of the Tasiapik River watershed are composed (from bottom to top) of frontal moraine sediments (gravel, pebbles, and stones), fluvioglacial sediments (sand and gravel), marine silts that contain permafrost mounds, and intertidal and littoral sand.

The Umiujaq region has a subarctic climate characterized by cool, humid summers and cold, dry winters, with a frost-free period of 60–80 days (Environment Canada 2004). The SILA network (VDTSILA) of the Centre d'études nordiques (CEN, Centre for northern studies) includes a meteorological station located in the Tasiapik Valley. This station recorded an average annual temperature of −3.1 °C between 2004 and 2018 (Centre d'études nordiques 2018). Between 2013 and 2017, the average annual precipitation in the region was 645 mm, of which approximately 50% was snow (Lemieux et al. 2020). The study region is in the discontinuous permafrost zone, where the permafrost is mainly found in palsas and lithalsas in the upstream and median parts of the valley. The surficial layer affected by freeze–thaw cycles is known as the active layer, which can reach an average thickness of 1.75 m in silty sand deposits and 3 m in sandy deposits (Fortier et al. 2020). Permafrost in this region is significantly impacted by the effects of climate change: between 1957 and 2005, the proportion of surface area occupied by lithalsas decreased by 40% (Fortier and Aube-Maurice 2008), with a 6% decrease between 2004 and 2009 (Beck et al. 2015). In addition, the degradation of permafrost between 1957 and 2005 led to a 175% increase in the proportion of land occupied by thermokarst lakes (Fortier and Aube-Maurice 2008).

The study region sits at the treeline, which extends south to this location due to the influence of Hudson Bay on the region's climate. The vegetation is characterized by a north–south delimitation, with shrub tundra in the east and forest tundra in the west (Payette 1983).

**Fig. 1.** Delimitation of the Tasiapik valley watershed as well as the locations of the turbidimeters installed in the river and the transects (source of the background image and hydrography: Ministère de l'Énergie et des Ressources naturelles (2019); Mapping tool: ArcGIS; Coordinate systems: NAD 83, MTM 9).

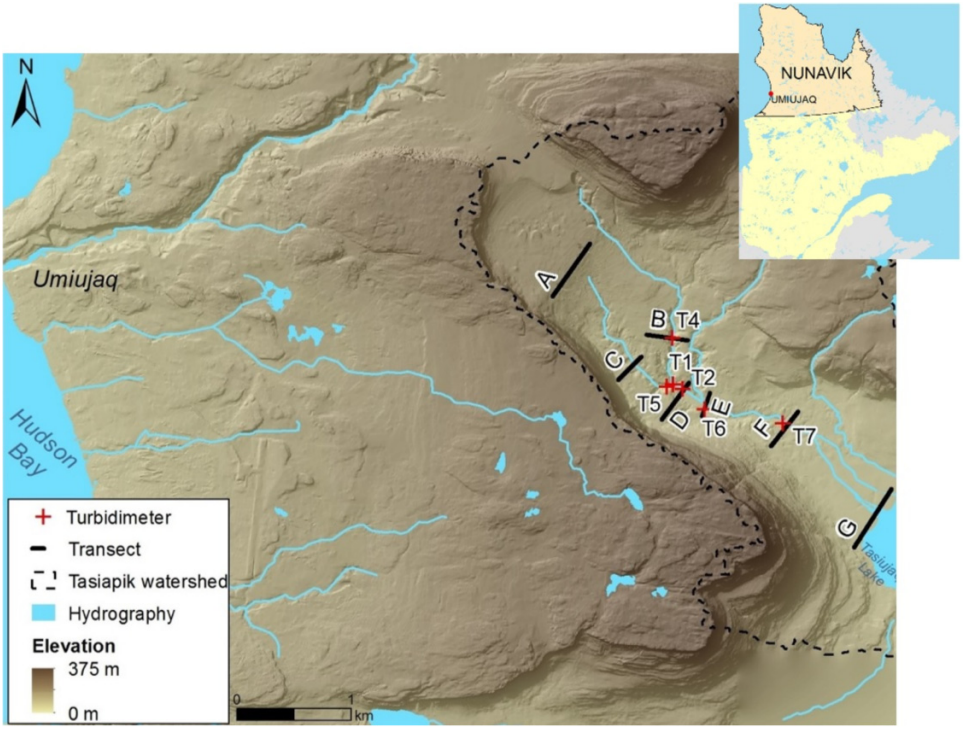


## Materials and methods

River systems are generally subdivided into three distinct zones: the source (or headwater) zone, the transition (or transfer) zone, and the floodplain (or depositional) zone (Schumm 1960, 1977). Erosion, transfer, and deposition occur in each zone, but the main processes generally shift from erosion upstream to deposition downstream (Miall 1977). For this research, all six turbidimeters were installed in the transfer zone. The headwater zone was unsuitable because the collection system (branches or tributaries) that collects and funnels water and sediment to the main stream is intermittent during the summer, while the rate of sedimentation in the depositional zone is high at this time, which causes the turbidimeters to become buried in sediment.

A turbidimeter was installed at each of the sites where transects perpendicular to the valley had been set up for topographic surveys (Fig. 1 and Supplemental Fig. 1). Turbidimeter 5 (T5) was installed in the upstream part of the river transfer zone within Transect C, which crosses permafrost mounds that are bare or weakly vegetated (lichen, *Betula glandulosa* Michx.). The river flows directly between mounds of permafrost which are approximately 2 m high. Turbidimeter 4 (T4) was installed in a tributary of the river within Transect B, originating from the northern part of the valley. A thin layer of silt sediment surmounts the bedrock at a relatively high elevation (about 20 m compared to the bed of the river), which results in a lack of permafrost. Turbidimeter 1 (T1) was installed at the confluence of the river and the tributary mentioned above, 60 m downstream from T5. Slightly downstream from this site, Transect D was established at the location of Turbidimeter 2 (T2). At this location, the banks are only 0.50 m high. The right bank consists of an alluvial plain approximately 70 m wide, extending to the foot of the permafrost mounds. The slope on the left bank is steeper due to the presence of a lithalsa that is gullied by the river. Turbidimeters 6 and 7 (T6, T7) were placed in the downstream part of the river in the transfer zone, with Transects E and F crossing both of these turbidimeters. In this area, the permafrost mounds are located several tens of meters from the river and are highly degraded (barely 0.40 m high). There are many thermokarst lakes here that are connected to the river by small streams. Two other transects were also established: one in the source zone (Transect A) and the other in the depositional zone (Transect G) (Supplemental Fig. 1).

The turbidimeters were manufactured by RBR Ltd. (model RBRsolo$^3$ Tu). This instrument uses an optical backscatter sensor method, which collects data in nephelometric turbidity units (NTU). The instruments were deployed using a wide plastic screen around the sensor to prevent organic material from interacting with the sensor. The deployment method also included a plastic device to protect the sensor from sunlight (Fig. 2). The instruments were stabilized on concrete blocks and placed in the river at a height of about 15 cm above the riverbed, with the sensor facing downstream (Fig. 2). The turbidimeters were programmed to record one measurement every 15 min during the frost-free period of the river, from June to October 2019.

**Fig. 2.** (*a*) Configuration for the installation of the turbidimeters during the summer of 2019. A screen (S) to retain the organic material and a plastic pallet (PP) were mounted on the turbidimeters (T) that were installed in concrete blocks placed on the riverbed. (*b*) Configuration for the installation of the turbidimeters during the summer of 2019. A screen (S) to retain the organic material and a plastic pallet (PP) were mounted on the turbidimeters (T) that were installed in concrete blocks placed on the riverbed.

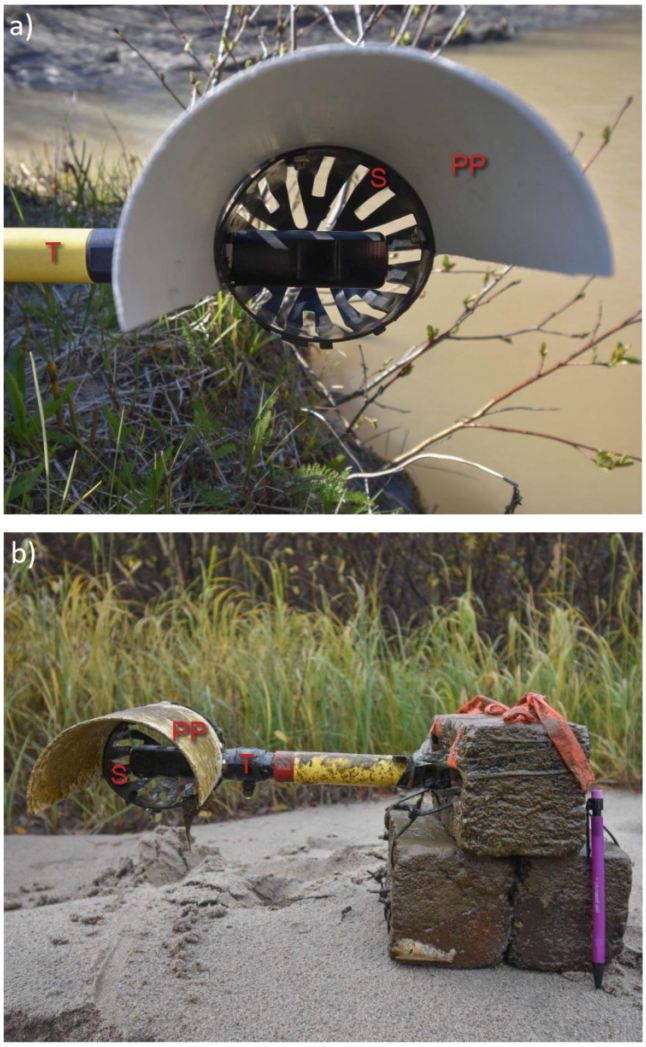




The turbidity data were analyzed in relation to the air temperature and precipitation data collected by CEN's environmental station VDTSILA, located upstream in the Tasiapik valley. The meteorological data were supplemented by measurements of the river flow rate that were collected by an automated gauging station. This system has been used in several studies on water resources in the valley (Lemieux et al. 2016; Cochand et al. 2019; Dagenais et al. 2020; Fortier et al. 2020; Lemieux et al. 2020). An automated camera was installed on the left bank of the river near T2 and was programmed to take a photograph every hour between 9:00 a.m. and 4:00 p.m. daily.

Statistical analyses were conducted to determine the relationship between the turbidity of the Tasiapik River and various parameters. All tests were performed using the statistical software *R*. Pearson correlation coefficients were calculated using the turbidity data from the river as a whole (a general calculation) as well as from each site separately. Several data sets were used to determine the relationships between variables at different time resolutions and in relation to different weather events. These included average daily measurements and hourly data over the entire season, as well as hourly data during warm periods and periods of high rainfall. The high rainfall periods were determined using the classification set by the Government of Canada (2019), where more than 7.6 mm/h corresponds to heavy rainfall. For air temperatures, warm temperatures were determined according to the standard deviation of the mean. To determine which parameter or combination of parameters had the most influence on variations in turbidity, model selection using the Akaike information criterion was performed. The AICTAB function of the AICcmodavg package was used to produce the collection results. The application conditions were checked before proceeding with the analyses; a Log + 1 transformation had to be applied to the turbidity response variable to adhere to the requirement for uniform variances. Following this analysis, a multi-model inference was carried out to determine the effect of each variable on turbidity.

Hysteresis loops were used to represent the relationship between the values of suspended sediment concentration (SSC, g/L) and the river flow rate (Q L/s) during a hydrological event. The SSC was determined with a field calibration where turbidity values and SSC measured at the same time were compared (Felix et al. 2018). Turbidity (Nephelometric Turbidity Unit; NTU) was converted to suspended sediment concentrations (g/L), using the following linear regression equation: $SSC = 1.5387 \times NTU + 9.1929$ (Manseau 2020). This characterization of sediment transport in rivers is illustrated graphically: we used the measurements of SSC and Q at the start of the hydrological event when the flow begins to increase, those at the end of the event when the flow returns to its low water-level value, in addition to measurements during the event. The graphs represent the variations of SSC (*y*-axis) and Q (*x*-axis) over time, weighted to 1, where 1 represents the maximum of SSC or Q reached during the event. The graph can be separated into two time periods: a rising limb, when the flow increases, and a falling limb, when the flow has reached its maximum and begins to decrease. The 12 events with the highest flow during the summer of 2019 were analyzed as part of this study. These 12 events were monitored using each of the six turbidimeters. Five classes of SSC–Q relation were identified, depending on the shape and orientation of the loop (Williams 1989; Tananaev 2015):

I. Type 1 is represented graphically by a line, where each SSC/Q ratio during the rising phase is equal to the SSC/Q ratio of the falling phase of the same flow measurement.
II. Type 2 is a clockwise loop, where the value of SSC in the rising phase is greater than the value of SSC during the downward phase of the same flow measurement. Two subtypes can be identified (a) when $SSC_{max}$ is reached before $Q_{max}$ and (b) when $SSC_{max}$ and $Q_{max}$ are observed simultaneously.

III. Type 3 is represented by a counterclockwise loop, where there is an increase in $SSC_{max}$ after $Q_{max}$. (This was observed relatively rarely).
IV. Hysteresis type 4, represented graphically by a line followed by a loop, combines type 1 with types 2 or 3.
V. Type 5 is represented by a figure eight loop that combines types 2 and 3.

## Results

The Tasiapik Valley covers a small watershed (12.25 $km^2$); nevertheless, it has a complex hydrographic network. The Tasiapik River originates from headwater streams on steep rocky slopes. The water then flows along intermittent streams encased in littoral sandy deposits. At certain points in the transfer zone, the river flows over fine sediments and between degrading permafrost mounds. In the downstream portion of the transfer zone, the river is fed by streams from nearby thermokarst lakes. Thus, several different sources of sediment transport are represented in the valley which produce different responses to the prevailing meteorological and flow conditions.

### Water turbidity and environmental conditions during the spring, summer, and fall

In 2019, the breakup of ice on the Tasiapik River occurred at the beginning of May, in contrast to the beginning of June in the previous year. Since the river was ice-free earlier than expected, the instruments were installed after the period of high-water levels following snow melt (from May 13 to June 22). Daily increases in turbidity occurred during the early summer from June 25 to 27 (Fig. 3) at all monitored sites, except at site T4. Maximum turbidity was recorded on June 25 (211 NTU at site T1). This period was characterized by very high air temperatures when compared to seasonal averages. These 3 days were among the five warmest days in the study period, with daily averages varying between 17.8 and 19.2 °C, including an hourly maximum of 25° C on June 27. Periods of increased river flow were also recorded on each day. We observed that the maximum flow rate reached on June 25 and 26 occurred a few hours after the maximum turbidity and air temperature were recorded. Correlation tests were carried out over this period to determine the relationship between turbidity and the various parameters (Table 1). The results show that there is a significant positive correlation between turbidity and air temperature at almost all of the sites ($r = 0.29$–$0.59$). High turbidity events are not generated by increased river flow, however, since discharge increased only after the peak of turbidity; this finding is also supported by the lack of correlation between flow and turbidity for most of the sites, except for sites T5 and T7.

An intense turbidity event occurred in the middle of the summer, while the maximum reached was recorded at all sites on July 16, ranging between 1118 NTU for T4 and 601 NTU for T1. The maximum flow rate was also recorded on that day with a peak of 413 L/s. This extreme runoff event was likely caused by the heavy rainfall that occurred a few hours earlier. July 16 was the rainiest day with 48 mm of precipitation, which corresponds to about 15% of the season's total precipitation. Figure 4 highlights the significant contribution of river flow to sediment transport dynamics during an extreme event such as this one. The severe precipitation event, which began at around 2:00 p.m., caused a sharp rise in river discharge which, in turn, led to an almost simultaneous increase in river turbidity. Turbidity and flow then decreased simultaneously after attaining their peak value.

Turbidity values recorded during different weather conditions were analyzed to better understand the effects of moderate and elevated precipitation levels on sediment transport. The results of the correlation tests (Table 2) show significant positive correlations (from a moderate to a strong degree) between precipitation and river turbidity ($r = 0.60$–$0.88$). The correlations were stronger when the analyses were only performed on data recorded during the periods of intense or moderate precipitation. For several events, increased turbidity and flow were observed several hours after the precipitation event. This finding led us to analyze the relationship between the turbidity of the river and the total precipitation that occurred in the hours preceding the turbidity recording, which is represented in Table 2 by the variable *P 24 h*. Using this previous 24 h time window, our data analysis revealed a significant increase in the strength of the correlation coefficient ($r = 0.66$) for most sites. For example, the Pearson correlation coefficient for T2 increased from 0.68 for the variable *P* to 0.88 for the variable *P 24 h*. These statistics show that during periods of moderate or heavy rainfall, the turbidity of the river and the total precipitation of the previous 24 h have a very strong positive correlation: turbidity increases with the increase in total precipitation (Fig. 4, Table 2).

Following the highest turbidity event recorded in the summer of 2019, turbidity remained relatively low and stable for a few weeks, except for a few isolated events (Fig. 5). From mid-August on, several successive increases in turbidity were recorded, particularly at site T2. For example, on August 9, the turbidity at this site increased to 169 NTU, while sites T4 and T7 only increased slightly and no variation was observed for sites T1, T5, and T6. For the 5 days preceding this event, daily air temperatures remained above the seasonal average, with a high of 15.5 °C recorded on August 8. This high turbidity event occurred during an increase in flow and an episode of moderate-intensity precipitation (5.7 mm over the 8 h preceding the increase). On August 15, an increase in turbidity was observed at site T2, reaching 238 NTU. This increase was also observed at site T5, with a maximum of 141 NTU, while the other turbidimeters did not record any significant increase. Air temperatures remained low in the days leading up to the event, as the amount of precipitation reached 9.7 mm in the preceding 5 h and the flow increased to 50 L/s. On August 19, the environmental station recorded slightly lower precipitation than during the previous event (7.1 mm in 5 h), but the flow was twice the rate recorded during the August 15 episode, with a maximum of more than 100 L/s. Air temperatures were warmer during this event, ranging between 12.7 and 15.6 °C for the previous 3 days. These weather and flow conditions resulted in increased turbidity at each site, varying between 88 and 133 NTU at sites T6 and T7, respectively.

**Fig. 3.** Recordings of the turbidity of the Tasiapik River at site T1, atmospheric temperatures, precipitation, and river flow during the warm period of June 25–27, 2019.

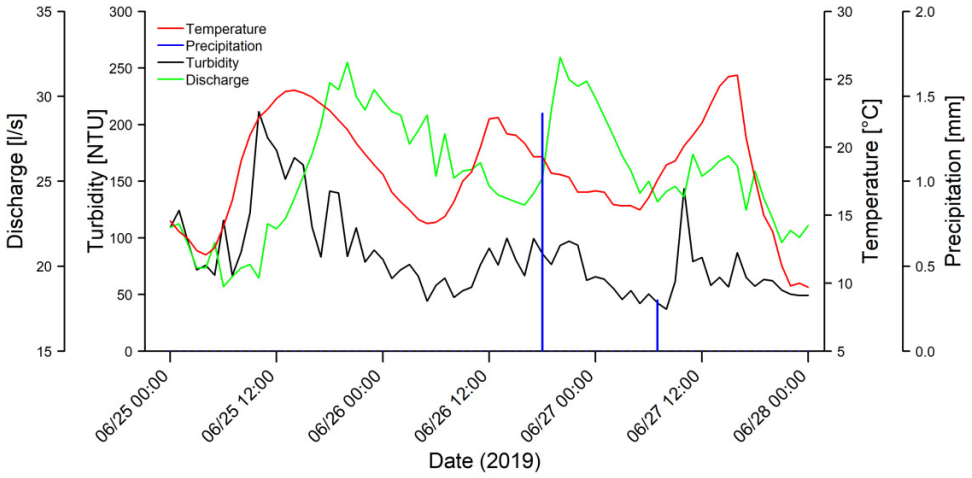


**Table 1.** Correlations between turbidity and air temperatures, precipitation, and discharge for the six stations installed in the summer of 2019 in the Tasiapik River.

| Site | Temperature | Precipitation | Discharge |
|---|---|---|---|
| | ° C | mm/h | l/s |
| T1 | **0.50∗∗∗** | -0.02 | -0.16 |
| T2 | **0.58∗∗∗** | -0.04 | 0.03 |
| T4 | 0.02 | -0.09 | 0.08 |
| T5 | **0.29∗** | -0.03 | **0.47∗∗∗** |
| T6 | **0.59∗∗∗** | -0.05 | 0.21 |
| T7 | **0.50∗∗∗** | 0.01 | **0.33∗∗** |

**Notes**: The data come from hourly records collected between June 25 and 27, 2019, when atmospheric temperatures remained relatively high. The results table includes the Pearson correlation coefficient for each of the relationships as well as the hypothesis tests: the indices in bold indicate a significant correlation ($p = 0$; $***p = 0.001$; $**p = 0.01$; $*p = 0.05$ ).

On August 31, 2019, a high turbidity event similar in magnitude to that of August 19 occurred, with maximum varying between 67 and 136 NTU. The total precipitation measured on that day was higher than that of August 19: 14.8 mm of rain in the 8 h preceding the event. However, river flow increased to a lesser extent during this episode, reaching a maximum of 70 L/s, as compared to 101 L/s on August 19. Air temperatures were below average the day before and were very low on the same day, with a daily average of 4.3 °C.

After this event, turbidity remained low until late summer. On September 22, 2019, the Tasiapik River experienced its second most significant turbidity event of the season, with maximum turbidity values between 185 NTU and 854 NTU at sites T4 and T6 respectively. These high values correspond to the second highest daily rainfall of the season totaling 43.2 mm, as recorded at the environmental station. It was also the second highest flow rate recorded in the summer of 2019, with a maximum of 335 L/s, while air temperatures had been below the average for 2 days.

## Correlation between turbidity, discharge, and environmental conditions during warm days

Correlation tests were performed on data recorded during warm days (>15 °C) throughout the season. The results indicate relatively high correlation coefficients between air temperatures and the turbidity of the Tasiapik River during the warm period between June 25 and 27. According to measurements taken on warm days during the study period (June–October 2019), the turbidity of the Tasiapik River and air temperatures varied in a similar way ($r = 0.26$) (Table 3). A statistical analysis of each of the sites separately showed that this relationship was quite strong for sites T1, T2, T6, and T7, while there was no significant correlation for sites T4 and T5. The strength of the correlation was greater for sites T2 and T6 ($r = 0.43$ and $r = 0.45$) than it was for sites T1 and T7 ($r = 0.36$ and $r = 0.26$). The results also indicate that there is no general correlation between precipitation and river turbidity when air temperatures are high. Site T5 is the only site where a significant relationship was observed between these two variables under such conditions, but in this case the strength of the coefficient was low ($r = 0.21$). There is a significant correlation between river flow and turbidity for this data set, which had also been observed in the results of the previous statistical analysis (Table 2).

## Model selection: parameters that regulate the variability of turbidity

A statistical model selection was made to determine which parameter or combination of parameters most influences the variation of turbidity. Fourteen candidate models were developed with the parameters used previously: (1) air temperatures, (2) precipitation, (3) river flow, (4) study site, (5) average air temperatures for the 48 h preceding the turbidity recording, and (6) total precipitation for the 24 h preceding the turbidity recording. The 14 candidate models used for model selection are presented in Table 4. The 24 h precipitation and discharge variables could not be included in the same model since these variables were correlated with each other. Tem-

**Fig. 4.** Recordings of the turbidity of the Tasiapik River at site T1, atmospheric temperatures, precipitation, and river flow during the period July 16–18, 2019.

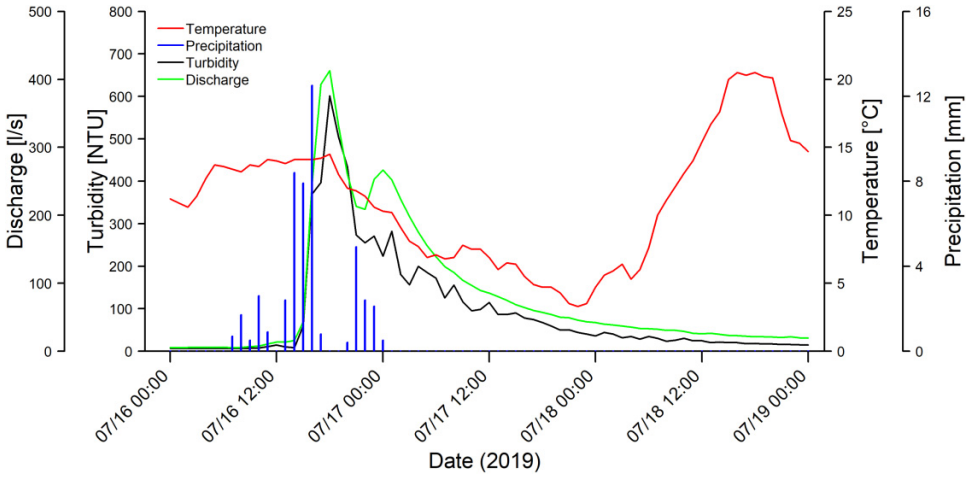


**Fig. 5.** Hourly data collected between June 24 and October 4, 2019 in the Tasiapik Valley: (*a*) mean atmospheric temperatures, (*b*) total precipitation, and (*c*) river flow, as well as turbidity at sites (*d*) T1, (*e*) T2, (*f*) T4, (*g*) T5, (*h*) T6, and (*i*) T7.

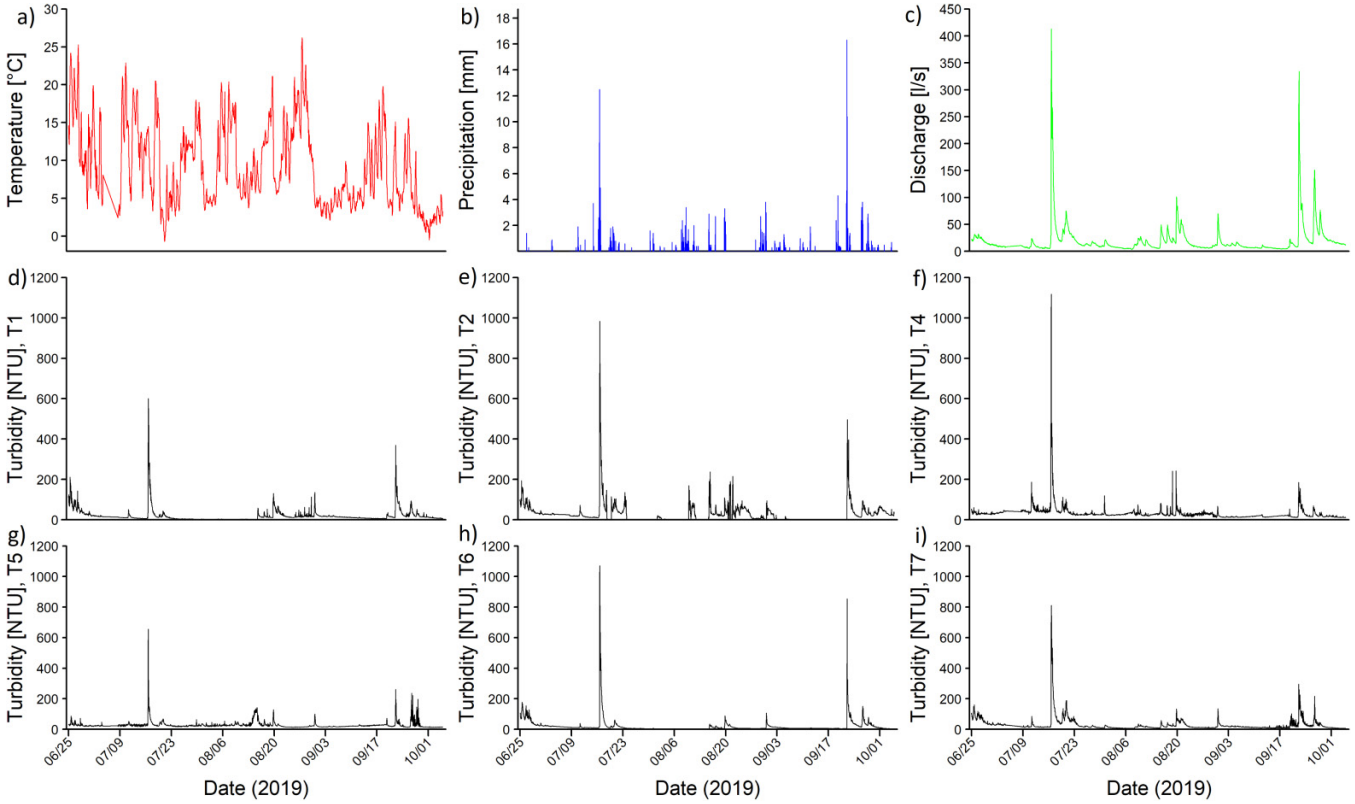


perature and 48 h temperature as well as precipitation and 24 h precipitation could also not be included in the same model.

Table 4 summarizes the results of the model selection. The results show that two models have a delta AICc ($\Delta i$) of less than 2, indicating that these models are highly plausible. These were model 10 (AICc = 17 648; $\Delta i = 0$), which includes the parameters of flow, 48 h temperature and site, and model 6 (AICc = 17 649; $\Delta i = 1.70$), which includes the parameters of precipitation, flow, 48 h temperature, and site. A multimodel inference was carried out on the parameters included in these two models, with a focus on the effect of the flow, 48 h temperature, and precipitation variables on the turbidity of the river. The results showed that the flow variable had an effect of 0.014 ± 0.001, with a 95% confidence interval of [0.013; 0.014]. Thus, there is a considerable effect of river flow on the turbidity of the water: for every 1 L/s increase in river flow, turbidity increased by 0.014 ± 0.001 NTU. The measure-

**Table 2.** Correlations between turbidity and air temperatures, precipitation, and flow for the Tasiapik River as well as for the six stations installed in the summer of 2019.

| Site | Temperature (° C) | Precipitation (mm/h) | 24 h precipitation (mm) | Discharge (L/s) |
|---|---|---|---|---|
| Tasiapik river | 0.17 | **0.50∗∗∗** | **0.66∗∗∗** | **0.74∗∗∗** |
| T1 | 0.14 | **0.50∗** | **0.80∗∗∗** | **0.92∗∗∗** |
| T2 | 0.18 | **0.68∗∗** | **0.88∗∗∗** | **0.94∗∗∗** |
| T4 | 0.19 | **0.46∗∗** | **0.61∗∗** | **0.58∗∗** |
| T5 | 0.16 | **0.58∗∗** | **0.67∗∗∗** | **0.78∗∗∗** |
| T6 | 0.29 | **0.75∗∗** | **0.73∗∗** | **0.86∗∗∗** |
| T7 | 0.11 | **0.46∗** | **0.77∗∗∗** | **0.93∗∗∗** |

**Notes:** The analyses were carried out on hourly data including only the periods of precipitation of moderate or strong intensity (>2.5 mm/h), collected between June 25 and October 4, 2019. The table of results includes the Pearson correlation coefficient for each of the relationships as well as the hypothesis tests: the indices in bold indicate a significant correlation ($p = 0$; $***p = 0.001$; $**p = 0.01$; $*p = 0.05$).

**Table 3.** Correlations between turbidity and air temperatures, precipitation, and flow for the entire Tasiapik River as well as for the six stations installed in the summer of 2019.

| Site | Temperature ° C | Precipitation mm/h | Discharge l/s |
|---|---|---|---|
| Tasiapik river | **0.26∗∗∗** | 0.02 | **0.56∗∗∗** |
| T1 | **0.36∗∗∗** | 0.04 | **0.59∗∗∗** |
| T2 | **0.43∗∗∗** | 0.02 | **0.65∗∗∗** |
| T4 | -0.01 | 0.03 | **0.21∗∗∗** |
| T5 | 0.05 | **0.21∗∗∗** | **0.56∗∗∗** |
| T6 | **0.45∗∗∗** | -0.07 | **0.65∗∗∗** |
| T7 | **0.26∗∗∗** | 0.01 | **0.77∗∗∗** |

**Notes:** Analyses were carried out on hourly data including only the temperature periods of high air temperatures (>15 °C), collected between June 25 and October 4, 2019. The table of results includes the Pearson correlation coefficient for each relationship as well as the hypothesis tests: the indices in bold indicate a correlation significant ($p = 0$; $***p = 0.001$; $**p = 0.01$; $*p = 0.05$).

ment associated with turbidity in this case is presented with a Log + 1 transformation, which was applied at the start of model selection. An effect of 0.028 ± 0.001 was observed with regard to the 48 h temperature variable, with a 95% confidence interval [0.026; 0.03]. The analysis shows that the average temperature of the 48 h preceding the turbidity measurement had an impact on the turbidity of the Tasiapik River. An increase in the Log + 1 turbidity of 0.028 ± 0.001 NTU was observed for each increase of 1 °C in the average air temperature. A multi-model inference was also produced with the precipitation variable since it was included in model 6. This parameter had an effect of 0.001 ± 0.004 with a 95% confidence interval [−0.007; 0.009].

### Hysteresis loops: the relationship between sediment concentration and discharge during the main hydrological events

A synthesis of the hysteresis loops observed at each site for the 12 hydrological events selected in the summer of 2019 is presented in Table 5, Fig. 6, and Supplemental Figs. 2a–f. The data show that the clockwise loops (type II) were the most commonly observed type in the river during the summer of 2019. For all of the sites except site T7, type II was the most frequently observed. Subtype IIa was recorded 33 times, compared to subtype IIb, which was recorded four times. Thus, in the Tasiapik River during summer 2019, most of the hydrological events were characterized by higher turbidity levels during the upward phase than during the downward phase, where $SSC_{max}$ was attained earlier than $Q_{max}$. The results also show that the type III hysteresis loops only occurred at three sites: at site T2 and the two sites downstream of this site (sites T6 and T7). The three sites located upstream of T2 did not record any counter-clockwise hysteresis loops. It is also interesting to note that site T7 recorded several type V loops, in contrast to the other sites. During the summer of 2019, this type of loop was observed nine times at the site. Sites T2 and T4 recorded this type of hysteresis five times. In addition, loop Type II was recorded the least often at site T7, with only one observation.

## Discussion

### Seasonal variation in turbidity: The case of site T4

Our results show that turbidity fluctuation is associated with river flow, but weather conditions prior to the event may contribute to the increase in turbidity in different ways, as demonstrated below using site T4 as an example.

Three of the increased turbidity events at site T4 occurred on different days (August 15, August 30–31, and September 26, 2019) and had similar turbidity levels: 83, 68, and 70 NTU. However, the meteorological conditions associated with these changes in turbidity were different (Fig. 7). For the first event on August 15 (Fig. 7*a*), maximum river turbidity was measured at 83 NTU and the flow was measured at 40 L/s. On this occasion, the rainfall had a rapid impact on turbidity, even though the precipitation was only of moderate intensity (9 mm over 5 h). The conditions preceding this date were very dry, with only 1.2 mm of rainfall in the preceding 92 h. Given these findings, it is reasonable to conclude that a large amount of available sediment was carried by the runoff wa-

**Table 4.** Parameters included in each of the candidate models used in model selection and results of the model selection presented as AICc table ranked from most likely to least likely model

| Model | Parameters | AICc rank | Log-*L* | AICc | Δ*i* | *wi* |
|---|---|---|---|---|---|---|
| Mod10 | Temperature + discharge + precipitation + site | 1 | −8814 | 17 648 | 0 | 0.70 |
| Mod6 | Temperature + Discharge + site | 2 | −8814 | 17 649 | 1.70 | 0.30 |
| Mod2 | Temperature + Precipitation + site | 3 | −9086 | 18 190 | 542 | 0 |
| Mod1 | Temperature + 24 h precipitation 24 h + site | 4 | −9085 | 18 191 | 543 | 0 |
| Mod8 | Temperature + site | 5 | −9170 | 18 359 | 711 | 0 |
| Mod11 | Precipitation + discharge + 48 h temperature + site | 6 | −9172 | 18 360 | 712 | 0 |
| Mod12 | Précipitation + température 48 h + site | 7 | −10 102 | 20 222 | 2574 | 0 |
| Mod4 | Precipitation + discharge + site | 8 | −10 232 | 20 483 | 2835 | 0 |
| Mod14 | Precipitation + site | 9 | −10 343 | 20 703 | 3055 | 0 |
| Mod7 | Discharge + 48 h temperature + site | 10 | −11 891 | 23 801 | 6153 | 0 |
| Mod13 | Discharge + site | 11 | −12 045 | 24 107 | 6459 | 0 |
| Mod3 | 48 h temperature + 24 h precipitation + site | 12 | −12 090 | 24 199 | 6551 | 0 |
| Mod9 | 48 h temperature + site | 13 | −12 091 | 24 199 | 6551 | 0 |
| Mod5 | 24 h precipitation + site | 14 | −12 253 | 24 522 | 6874 | 0 |

**Table 5.** Summary of hysteresis loops observed in the Tasiapik River during summer 2019.

| Site | Hysteresis loop type | Number of observations |
|---|---|---|
| T1 | IIa | 7 |
| | IIb | 1 |
| | IV | 1 |
| | V | 3 |
| T2 | IIa | 6 |
| | IIIa | 1 |
| | V | 5 |
| T4 | IIa | 7 |
| | V | 5 |
| T5 | IIa | 5 |
| | IIb | 3 |
| | V | 4 |
| T6 | IIa | 7 |
| | IIIa | 3 |
| | V | 2 |
| T7 | IIa | 1 |
| | IIIa | 2 |
| | V | 9 |

**Notes:** The table shows the number of loops observed at each of the six sites, according to the type of hysteresis.

ter that entered the river. The second event on August 30–31 (Fig. 7*b*) had a slightly lower maximum turbidity (68 NTU), but the river flow was almost double that of the preceding event noted above. The flow reached 70 L/s, with 15 mm of rainfall. The difference is even more noticeable in the third case on September 26 (Fig. 7*c*). The flow on this day was almost four times higher than the first event and twice as much as the second, with a maximum of 151 L/s. This increased flow was one of the highest of the season and was caused by medium-intensity precipitation over a long period: 30 mm of rain over 13 h. Nevertheless, despite these more intense conditions, the turbidity remained similar to the previous events, reaching a maximum of 70 NTU.

Therefore, it appears that during mid-August, when summer conditions predominated (dry conditions illustrated by very little rain and a low river flow rate), reduced precipitation mobilized the non-cohesive surface sediments and triggered an increase in turbidity. Toward the end of the summer (August 30–31) and at the beginning of the fall (September 26), the amount of rain increased significantly, favoring an increase in flow and a subsequent increase in turbidity.

## Variations in turbidity and triggering factors

Sediment transport in rivers is highly dependent on water flow and meteorological parameters. However, local environmental factors such as the geology and geomorphology of the watershed, surface deposits, the layout of the river, the quality of the soil and vegetation, etc., can amplify or minimize the impact of these parameters by causing variations in the turbidity in each section of a river (Douglas 1967; Wilson 1973; Milliman and Syvitski 1992; Syvitski 2002). Based on our data analysis and field observations, these factors include mass movements, thermokarst processes, groundwater flow in discontinuous permafrost environments, and spring precipitation.

## Mass movements

The sediment load of rivers at high latitudes is generally determined by geomorphological processes occurring during periods of higher air temperature. One of the primary causes of sediment input into rivers in permafrost environments is mass movement on the riverbank (Lewis et al. 2005; Lewkowicz and Harris 2005; Lamoureux and Lafrenière 2009; Jolivel and Allard 2017). At our study site, by analyzing photographs taken with an automatic camera installed at site T2 (Supplemental Figs. 3a, b), we were able to observe several mass movements along the river during the summer of

**Fig. 6.** Different types of hysteresis loops observed in the Tasiapik river during the summer of 2019. Data are presented as normalized values; 1 represents the maximum value reached during the event, and 0 is the minimum value. (*a*) Type IIa observed at T2 on August 17; (*b*) type IIb observed at T5 on August 19–20; (*c*) type III observed at T6 on July 20–21; (*d*) type IV observed at T1 on July 20–21; (*e*) type V observed at T4.

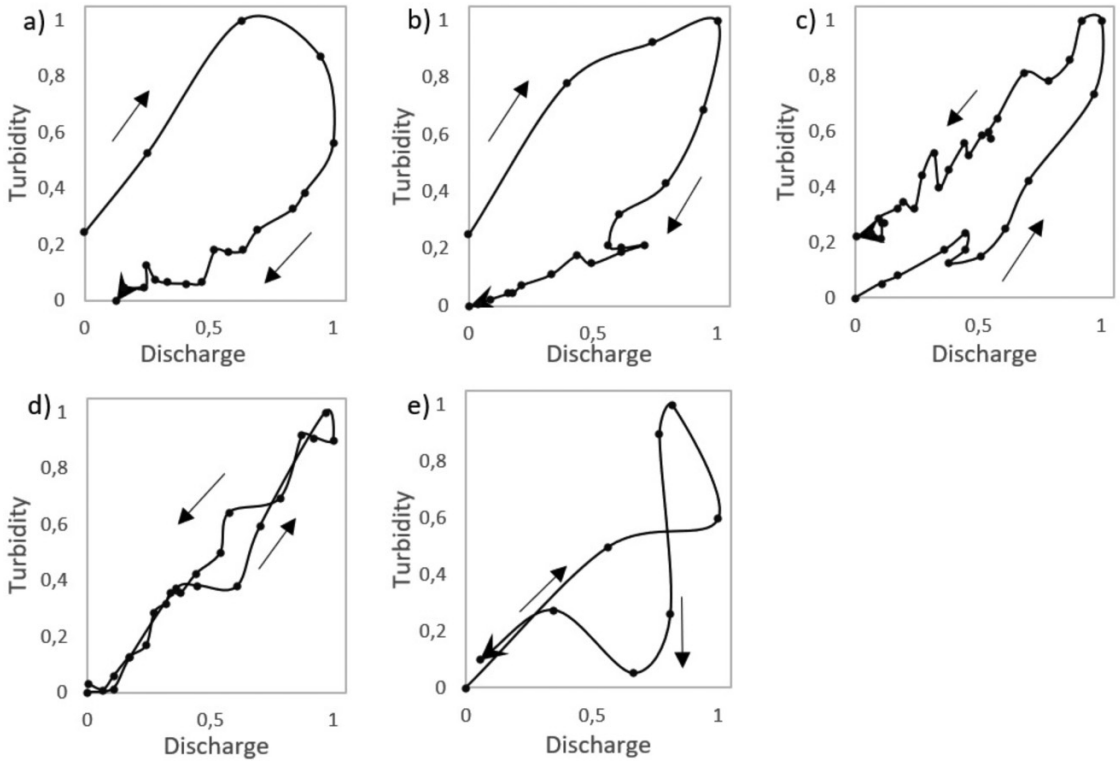




2019. The most significant events were produced at the end of the spring following the snow melt. June 9 and 10 were unusually hot days in the Tasiapik Valley, reaching a maximum of 28.8 °C on June 10. A rainy period resulting in 23.7 mm of precipitation was recorded at the VDTSILA meteorological station on June 11. The combination of these two types of conditions (warm and rainy) led to very strong fluvial erosion of the lithalsa edges, which was observed in the photographs (Supplemental Figs. 3a, b). The rapid mass movement would have resulted from the detachment of the active layer, which is caused by the deepening of the active layer after periods of elevated air temperature (Lewkowicz 1990). According to Lewis et al. (2005), even just one such event may cause more than 30% of the total sediment transport in a river during the spring. Along the Tasiapik River, the second event occurred on June 16, when 12 mm of rain was recorded. As with the first event, air temperatures were above average for the two preceding days, reaching a maximum of 16 °C. By comparing the photographs from June 7 to June 19, we observed that most of the sediment had accumulated on the riverbed near site T2. Unfortunately, these observations could not be confirmed by the turbidity data because the turbidimeters were only installed on June 25. Such mass movements affected the banks of the Sheldrake River about 12 km further north on May 6, 2010, leading to a considerable increase in turbidity from ~5 NTU to 22 NTU (Jolivel and Allard 2017).

The accumulation of sediment at the base of the lithalsa did not increase much during the remainder of the season, even after periods of intense precipitation and increased flow. The photographs showed that more sediment was deposited after the snow melt than during the summer or at the end of the summer. This could be explained by the fact that the active layer thaws more rapidly in the spring. This interpretation is supported by French (2007), who found that 75% of the thaw in periglacial environments occurs during the first 5 weeks after the air temperature increases to above 0 °C. The warm periods increase the depth of the active layer of the permafrost, causing instability on the banks, facilitating erosion, and triggering mass movements. The sediments become available and are then transported toward the river during periods of intense precipitation or during increased river flow.

The statistical analysis carried out for periods in which the air temperature was higher (Table 3) revealed a significant correlation between river turbidity and air temperature, with a medium to strong correlation ($r = 0.43$). The highest correlation between these conditions was found at site T6 ($r = 0.45$), which is located approximately 200 m downstream of site T2. The correlation coefficients were even stronger when data from June 25 to 27 were used, one of the hottest periods of the summer of 2019; the coefficient for site T2 was $r = 0.58$ and for site T6 it was $r = 0.59$ (Table 1). These findings are consistent with studies by Lewkowicz and Harris (2005) on

**Fig. 7.** Hourly data of atmospheric temperature and precipitation collected in the Tasiapik Valley as well as river flow and turbidity data collected at site T4

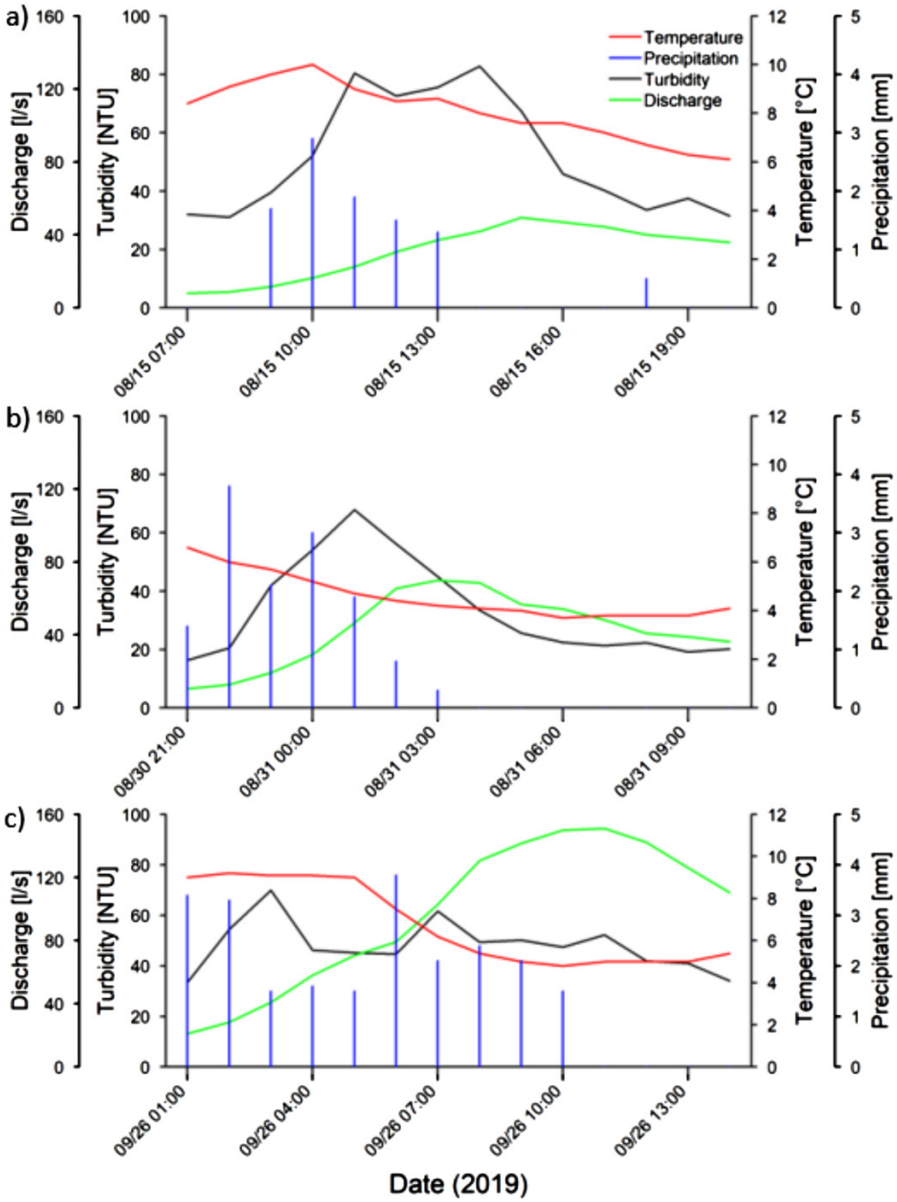


Ellesmere Island (Nunavut, Canada), which found that minimum thresholds of daily sunlight and air temperature were required to trigger mass movements. An increase in air temperature in environments at high latitudes causes an increase in mass movements and increased turbidity.

## Thermokarst processes

Thermokarst lakes that formed as a result of degradation of lithalsas or palsas can also contribute to increased river turbidity. Several of these thermokarst lakes are in the downstream section of the transfer zone in the Tasiapik Valley. Some are located downstream of site T7 and are connected to the Tasiapik River by small channels. The hysteresis loop data indicate that the dynamics of sediment transport are largely influenced by thermokarst processes. Type V loops were frequently observed at site T7, indicating a combination of different sources of sediment generated by transport from tributaries or the collapse of riverbanks. No mass movements were observed on the banks near site T7; the closest was more than 600 m upstream, near site T2. Sediment transport from thermokarst ponds is the most likely hypothesis for the many type V events found here. Moreover, the small number of type II loops observed at this site indicate that the sediment source is not located near the study site. This supports the findings of Jolivel and Allard (2013), who linked the 160% increase in sediment transport recorded in the Sheldrake River to the increase in connectivity between the thermokarst ponds. In fact, increases in the size and quantity of thermokarst ponds can create a network of interconnecting channels (Seguin and Allard 1984) that facilitate sediment transport toward the river. Bowden et al. (2008) also demonstrated that the concentration of suspended sediments in the Toolik River was two

times higher downstream of the thermokarst ponds than in the upstream portion of the river.

The contribution of sediment to the Tasiapik River from thermokarst ponds is also indicated by the accumulation of sand at the mouth of tributaries originating from these ponds (Supplemental Fig. 4). During periods of intense precipitation, the increase in the water level of the ponds disperses sediment-laden water into the Tasiapik River, as was observed during fieldwork in the summer of 2019. These findings show that the ponds formed by the degradation of permafrost, which has been occurring to a higher degree in the Tasiapik Valley over the last few decades (Fortier and Aube-Maurice 2008), are a non-negligible source of sediment transport in the hydrographic network of the Tasiapik Valley.

## Flow

On June 25–27, 2019, the flow rate of the Tasiapik River was high (about 10 L/s). The maximum flow was recorded as occurring 2–3 h after the maximum temperature had been reached on those days. These increases in river flow observed during the hottest days of the summer of 2019 led to significant increases in turbidity. This concords with several studies conducted on rivers in permafrost environments that showed that the river flow during the spring is largely controlled by the temperature pattern of the catchment area (Michel and Van Everdingen 1994; Syvitski 2002; Forbes and Lamoureux 2005). In fact, according to Syvitski (2002), an increase of 2 °C in air temperature in a watershed combined with a 20% increase in river flow can cause a 32% increase in the sediment load of an arctic river. This variation in turbidity is dependent on the ground thaw rate and snow melt, and it was observed more often when air temperatures and solar radiation were high (Kokelj et al. 2013).

In addition, observations from all of the sites (except for site T4, which is not located near a lithalsa) revealed a significant and relatively strong correlation between turbidity and air temperature during warm periods ($r = 0.29$ for site T5 and $r = 0.59$ for site T6). By contrast, significant correlations between turbidity and flow were only observed for sites T5 and T7 ($r = 0.47$ and $r = 0.33$ respectively). Diurnal variations of flow and turbidity were also observed in studies of the Mackenzie and Peel Rivers (Northwest Territories, Canada), where turbidity ranged between 200 NTU from 2 am to 12 pm and 1200 NTU several hours after the daily maximum of sunlight (Kokelj et al. 2013). This level of turbidity was considerably higher than was observed in the Tasiapik River, which has a much smaller watershed: the maximum between June 25 to 27, 2019, was 211 NTU.

## Precipitation

The statistical results indicate that sites T4 and T5 were more affected by precipitation. After analyzing the results from correlation tests using daily averages, site T5 was the only one in which the Pearson coefficient was higher for precipitation ($r = 0.71$) than for flow ($r = 0.68$). Sediment transport in the downstream portion of the transport zone is influenced by the existing topography (steep riverbanks), which enhances the flow of surface runoff and facilitates the transport of sediment to the river. In addition, the rapid and deep melting of the ice in the permafrost increased soil humidity. When the capacity of the soil to retain water derived from precipitation was reduced, surface runoff toward the river increased. Similar conditions were also observed in Cape Bounty (Melville Island, Nunavut, Canada) and led to a total suspended sediment load equivalent to 35% of the total for the summer season as a whole over only two days of precipitation (Dugan et al. 2009).

The correlation tests that only included periods of elevated air temperature (Table 3) showed that turbidity and precipitation varied in a similar manner at site T5 ($r = 0.21$). Following the thawing of the soil in summer, the sediment becomes available for transport due to soil compaction, the activation of ostioles, and slight detachments from the active layer. During a precipitation event, sediment is taken up by surface runoff and transported toward the river, causing an increase in turbidity. At site T5, an event occurred on August 31 that increased turbidity to a maximum of ~100 NTU. This event appears to be related to this process, since the five previous days were relatively warm, with daily average temperatures between 13 and 20 °C. In similar circumstances, Dugan et al. (2009) observed an increase in turbidity to more than 60 NTU in a river on Melville Island (Nunavut). This event was linked to sedimentary transport from surface runoff after a precipitation event during a period of elevated air temperatures.

Hence, our study found a positive correlation between turbidity and precipitation for all of the study sites on the Tasiapik River. However, the relationship is stronger when the data set only includes periods of precipitation of moderate to strong intensity. These findings indicate that a certain amount of precipitation is necessary to create sufficient levels of surface runoff to load and transport sediment toward the river and increase turbidity over a short time span. As was observed in the Boothia Peninsula (Nunavut, Canada), even periods of light precipitation can provide sufficient quantities of water to infiltrate the soil and create surface runoff (Forbes and Lamoureux 2005). However, such quantities of rain were not sufficient to increase flow to a level that could cause the erosion of material from the banks or the riverbed. When precipitation is more intense, as determined over the preceding 24-h period of cumulative precipitation data, the force coefficient of the correlation increases significantly. Weak-intensity precipitation over a long period may also be sufficient to increase the flow rate and thereby increase river turbidity. As seen in the work of Göransson et al. (2013) in Sweden's Göta Älv River, there is a lag between precipitation episodes and the increase of turbidity and flow in the river. A study by Hamilton and Luffman (2009) of the Little River in Tennessee also found a higher correlation between precipitation and turbidity within a 24-h window. This time interval may be more or less significant depending on specific geomorphological characteristics of the study region such as the size of the watershed and the type of surface deposits.

# Conclusion

This study has provided evidence of the significant effects of meteorological conditions and the relevant hydro-

morphological characteristics of the watershed on variations in turbidity in the Tasiapik River (Nunavik, Canada), which is located in a discontinuous environment. Our results showed that following an increase in flow rate, there was an almost simultaneous increase in turbidity due to the erosion of the banks and the suspension of sediment from the riverbed. The duration and intensity of precipitation events are also important factors affecting the process of sediment transport in rivers. A threshold amount of precipitation is necessary to trigger surface runoff to a sufficient degree that will cause loose deposits to be taken up and transported to the river.

This study also examined whether variations in turbidity in the Tasiapik River were linked to permafrost degradation resulting from an increase in the air temperature. The statistical analysis indicated that turbidity was influenced by the air temperature. The force of the correlation coefficient increases in a significant manner when the tests only focus on the warmest periods (June 25–27, 2019) ($r = 0.5$). The results obtained from the selection of statistical models also indicated that air temperature had an influence on turbidity in the Tasiapik River because both of the plausible models included the variable of temperature.

Even though meteorological conditions and flow rate are important factors affecting turbidity in the Tasiapik River, hydrographic networks in high latitude regions are complex systems that are uniquely influenced by permafrost in addition to other factors. In the Tasiapik Valley, the degradation of permafrost mounds created thermokarst ponds that act as sediment wells. The sediment is transported to the river along a gulley network. Mass movements on the banks of the river also create instability due to the deepening of the active layer of permafrost, directly contributing to the increased turbidity of the Tasiapik River by freeing loose deposits for transport.

While this study of the Tasiapik River gives us more insight into the evolution of turbidity in rivers at high latitudes, it would be beneficial to conduct a similar study over a longer period of time. Other parameters such as the rate of soil thaw and the quantity of snow accumulated during the previous winter should also be included in the analysis. Snow accumulation, in particular, could play an important role in the dynamics of sediment transport in rivers.



## Acknowledgements

Funding for this project was provided by the Sentinel North program, financed by the Canada First Research Excellence Fund (CFREF), CRNSG-RGPIN-2020–06699 (Najat Bhiry), and CRSNG- RGPIN-2019–05188 (John Molson). Thanks are extended to the community of Umiujaq for its ongoing support. The authors also want to thank Richard Fortier, Jean-Michel Lemieux, and their team for providing us with the flow data as well as Denis Sarrazin and Madiha Khadhraoui for their valuable help in the field, the Northern Scientific Training Program, and the Centre d'études nordiques (CEN) for logistical support.

## Article information

### History dates

Received: 19 July 2021
Accepted: 9 March 2022
Accepted manuscript online: 13 April 2022
Version of record online: 12 September 2022

### Notes

This paper is part of a Collection entitled "Terrestrial Geosystems, Ecosystems, and Human Systems in the Fast-Changing Arctic".

### Copyright



## Supplementary material

Supplementary data are available with the article at https://doi.org/10.1139/as-2021-0036.

## References

Banville, D.R. 2016. Modélisation cryohydrogéologique tridimensionnelle d'un bassin versant pergélisolé: une étude cryohydrogéophysique de proche surface en zone de pergélisol discontinu à Umiujaq au Québec nordique [Three-dimensional cryohydrogeological modeling of a permafrost watershed: a near-surface cryohydrogeophysical study in the discontinuous permafrost zone at Umiujaq in northern Quebec]. MSc Thesis, Université Laval, Quebec City, QC, 278pp.

Beck, I., Ludwig, R., Bernier, M., Lévesque, E., and Boike, J. 2015. Assessing permafrost degradation and land cover changes (1986-2009) using remote sensing data over Umiujaq, sub-arctic Québec. Permafrost and Periglacial Processes, **26**: 129–141. doi:10.1002/ppp.1839.

Bense, VF., Ferguson, G., and Kooi, H. 2009. Evolution of shallow groundwater flow systems in areas of degrading permafrost. Geophysics Research Letters, **36**(22): L22401. doi:10.1029/2009GL039225.

Bowden, W.B., Gooseff, M.N., Balser, A., Green, A., Peterson, B.J., and Bradford, J. 2008. Sediment and nutrient delivery from thermokarst features in the foothills of the north slope, Alaska: potential impacts on headwater stream ecosystems. Journal of Geophysical Research Biogeosciences, **113**: 1–12. doi:10.1029/2007JG000470.

Brown, R., Lemay, M., Allard, M., Barrand, E.N., Barette, C. Bégin, Y., et al. 2012. Climate variability and change in the Canadian Eastern Subarctic IRIS region. Edited byAllard and Lemay, In Nunavik and Nunatsiavut: From science to policy. An Integrated Regional Impact Study (IRIS) of climate change and modernisation, Québec, QC, pp. 57–113.

Centre d'études nordiques. 2018. Données des stations climatiques d'Umiujaq au Nunavik, Québec, Canada. doi: https://doi.org/10.5885/45120SL-067305A53E914AF0.

Chandler, F.W. 1988. The early Proterozoic Richmond Gulf graben, east coast of Hudson Bay, Quebec. Geological Survey of Canada, Ottawa, Canada.

Cochand, M., Molson, J., and Lemieux, J.M. 2019. Groundwater hydrogeochemistry in permafrost regions. Permafrost and Periglacial Processes, **30**: 90–103. doi:10.1002/ppp.1998.

Cochand, M., Molson, J., Barth, J.A.C., van Geldern, R., Lemieux, J.M., and Fortier, R., 2020. Rapid groundwater recharge dynamics determined from hydrogeochemical and isotope data in a small permafrost watershed near Umiujaq (Nunavik, Canada). Hydrogeology Journal, **28**: 853–868. doi: 10.1007/s10040-020-02109-x.

Cumming, H., and Herbert, N.A. 2016. Gill structural change in response to turbidity has no effect on the oxygen uptake of a juvenile sparid fish. Conservation Physiology, **4**: cow033. doi:10.1093/conphys/cow033. PMID: 27766155.

Dagenais, S., Molson, J., Lemieux, J.M., Fortier, R., and Therrien, R. 2020. Coupled cryo-hydrogeological modelling of permafrost dynamics near Umiujaq (Nunavik, Canada). Hydrogeology Journal, **28**: 887–904. Springer. doi:10.1007/s10040-020-02111-3.

Douglas, I. 1967. Man, vegetation and the sediment yields of rivers. Nature, **215**: 925–928. doi:10.1038/215925a0.

Dugan, H.A., Lamoureux, S.F., Lafrenière, M.J., and Lewis, T. 2009. Hydrological and sediment yield response to summer rainfall in a small high arctic watershed. Hydrological Processes, **23**: 1514–1526. doi:10.1002/hyp.7285.

Eaton, D.W., and Darbyshire, F. 2010. Lithospheric architecture and tectonic evolution of the Hudson Bay region. Tectonophysics, **480**: 1–22. doi:10.1016/j.tecto.2009.09.006.

Environnement Canada. 2004. Canadian climate normals or averages 1971-2000. Environnement Canada, Ottawa, Canada.

Favaro, E.A., and Lamoureux, S.F. 2015. Downstream patterns of suspended sediment transport in a high arctic river influenced by permafrost disturbance and recent climate change. Geomorphology, **246**: 359–369. doi:10.1016/j.geomorph.2015.06.038.

Felix, D., Albayrak, I., and Boes, R.M. 2018. In-situ investigation on real-time suspended sediment measurement techniques: turbidimetry, acoustic attenuation, laser diffraction (LISST) and vibrating tube densimetry. International Journal of Sediment Research, **33**: 317. doi: https://doi.org/10.1016/j.ijsrc.2017.11.003.

Forbes, A.C., and Lamoureux, S.F. 2005. Climatic controls on streamflow and suspended sediment transport in three large middle arctic catchments, Boothia Peninsula, Nunavut, Canada. Arctic, Antarctic, and Alpine Research, **37**: 304–315. doi:doi:10.1657/1523-0430(2005)037[0304:CCOSAS]2.0.CO;2.

Fortier, R., and Aube-Maurice, B. 2008. Fast permafrost degradation near Umiujaq in Nunavik (Canada) since 1957 assessed from time-lapse aerial and satellite photographs. *In* International Conference on Permafrost (ICOP) Proceedings, Quebec City, QC, Canada. **Vol. 9**, pp. 457–462. Available at: https://www-engineeringvillage-com.acces.bibl.ulaval.ca/search/doc/abstract.url?&pageType=quickSearch&usageZone=resultslist&usageOrigin=searchresults&searchtype=Quick&SEARCHID=ffe718d3M20eeM4866M8ebaM2529bc538435&DOCINDEX=1&ignore_docid=grf_M578b2cf614856 [accessed 25 April 2020].

Fortier, R., Banville, D.R., Lévesque, R., Lemieux, J.M., Molson, J., and Therrien, R., 2020. Development of a three-dimensional geological model, based on quaternary chronology, geological mapping, and geophysical investigation, of a watershed in the discontinuous permafrost zone near Umiujaq (Nunavik, Canada). Hydrogeology Journal, **28**: 813–832. doi:10.1007/s10040-020-02113-1.

French, H.M. 2007. Present-day periglacial environments. *In* The periglacial environment, 3rd ed. John Wiley and Sons, Chichester, UK. pp. 47–82.

Göransson, G., Larson, M., and Bendz, D. 2013. Variation in turbidity with precipitation and flow in a regulated river system-river Göta Älv, SW Sweden. Hydrology and Earth System Sciences, **17**: 2529–2542. doi:10.5194/hess-17-2529-2013.

Government of Canada. 2019. Glossary. Availabale from https://climate.weather.gc.ca/glossary_f.html [accessed 20 April 2020].

Haeberli, W., and Hohmann, R. 2008. Climate, glaciers, and permafrost in the Awiss Alps 2050: scenarios, consequences and recommendations. *In* 9th International Conference on Permafrost. 29 June - 3 July 2008. Fairbanks, AK, USA. pp. 607–612. doi:10.5167/uzh-6025.

Hamilton, J.L., and Luffman, I. 2009. Precipitation, pathogens, and turbidity trends in the Little River, Tennessee. Physical Geography, **30**: 236–248. doi:10.2747/0272-3646.30.3.236.

Holloway, J.E., and Lewkowicz, A.G. 2020. Half a century of discontinuous permafrost persistence and degradation in Western Canada. Permafrost and Periglacial Processes, **31**: 85–96. doi:10.1002/ppp.2017.

IPCC 2014. Climate Change 2014: synthesis report. Contribution of working groups I, II and III to the Fifth Assessment Report of the Intergovernmental Panel on Climate Change. IPCC. Geneva, Switzerland. doi:10.1017/CBO9781107415324.

Jolivel, M., and Allard, M. 2013. Thermokarst and export of sediment and organic carbon in the Sheldrake River watershed, Nunavik, Canada. Journal of Geophysical Research Earth Surface, **118**: 1729–1745. doi:10.1002/jgrf.20119.

Jolivel, M., and Allard, M. 2017. Impact of permafrost thaw on the turbidity regime of a subarctic river: the Sheldrake River, Nunavik, Quebec. Arctic Science, **3**: 451–474. doi:10.1139/as-2016-0006.

Kokelj, S.V., Lacelle, D., Lantz, T.C., Tunnicliffe, J., Malone, L., and Clark, I.D., 2013. Thawing of massive ground ice in mega slumps drives increases in stream sediment and solute flux across a range of watershed scales. Journal of Geophysical Research Earth Surface, **118**: 681–692. doi:10.1002/jgrf.20063.

Lamoureux, S.F., and Lafrenière, M.J. 2009. Fluvial impact of extensive active layer detachments, Cape Bounty, Melville Island, Canada. Arctic, Antarctic, and Alpine Research, **41**: 59–68. doi:10.1657/1938-4246(08-030)[LAMOUREUX]2.0.CO;2.

Lavoie, C., Allard, M., and Duhamel, D. 2012. Deglaciation landforms and C-14 chronology of the lac Guillaume-Delisle area, eastern Hudson Bay: a report on field evidence. Geomorphology **159–160**: 142–155. dois. doi:10.1016/j.geomorph.2012.03.015.

Lemieux, J.-M., Fortier, R., Talbot-Poulin, M.-C., Molson, J., Therrien, R. Ouellet, M., et al. 2016. Groundwater occurrence in cold environments: examples from Nunavik, Canada. Hydrogeology Journal, **24**: 1497–1513. doi:10.1007/s10040-016-1411-1.

Lemieux, J.M., Fortier, R., Murray, R., Dagenais, S., Cochand, M. Delottier, H., et al. 2020. Groundwater dynamics within a watershed in the discontinuous permafrost zone near Umiujaq (Nunavik, Canada). Hydrogeology Journal, **28**: 833–851. 10.1007/s10040-020-02110-4. doi:

Lewis, T., Braun, C., Hardy, D.R., Francus, P., and Bradley, R.S. 2005. An extreme sediment transfer event in a Canadian High Arctic stream. Arctic, Antarctic, and Alpine Research, **37**: 477–482. doi:doi:10.1657/1523-0430(2005)037[0477:AESTEI]2.0.CO;2.

Lewkowicz, A.G. 1990. Morphology, frequency and magnitude of active layer detachment slides, Fosheim peninsula, Rllesmere Island, N.W.T. Nordicana, **54**: 111–118.

Lewkowicz, A.G., and Harris, C. 2005. Frequency and magnitude of active-layer detachment failures in discontinuous and continuous permafrost, northern Canada. Permafrost and Periglacial Processes, **16**: 115–130. doi:10.1002/ppp.522.

Manseau, F. 2020. La turbidité de la rivière Tasiapik (Umiujaq, Nunavik) en lien avec la dégradation du pergélisol. MSc thesis, Université Laval, Quebec City, QC, 105 pp.

McKenzie, J.M, and Voss, C.I. 2013. Permafrost thaw in a nested groundwater flow system. Hydrogeology Journal, **21**(1): 299–231. doi:10.1007/s10040-012-0942-3.

Miall, A.D. 1977. Fluvial sedimentology. Canadian Society of Petroleum Geologists, Calgary, Canada.

Michel, F.A., and Van Everdingen, R.O. 1994. Changes in hydrogeologic regimes in permafrost regions due to climatic change. Permafrost and Periglacial Processes, **5**: 191–195. doi:10.1002/ppp.3430050308.

Milliman, J.D., and Syvitski, J.P.M. 1992. Geomorphic/tectonic control of sediment discharge to the ocean: the importance of small mountainous rivers. Journal of Geology, **100**: 525–544. doi:10.1086/629606.

Minello, T.J., and Benfield, M.C. 2018. Effects of turbidity on feeding of southern flounder on estuarine prey. Marine Ecology Progress Series, **594**: 203–212. doi:10.3354/meps12535.

Ministère de l'Énergie et des Ressources naturelles. 2019. Cartes topographiques des villages autochtones du nord à l'échelle de 1 /2 000. Direction générale de l'information géospatiale, Québec, Québec, Canada. Available from https://www.donneesquebec.ca/recherche/dataset/cartes-topographiques-des-villages-autochtones-du-nord-a-lechelle-de-1-2-000 [accessed 25 April 2020].

Ouranos 2015. Vers l'adaptation. Synthèse des connaissances sur les changements climatiques au Québec. Partie 1: Évolution climatique au Québec; Ouranos, Montréal, Québec.

Payette, S. 1983. The forest tundra and present tree-lines of the northern Quebec-Labrador Peninsula. *In:* Proceedings of the northern Quebec tree-line conference. Collection Nordicana, Québec, QC, pp. 3–24.

Ran, Y., Li, X., and Cheng, G. 2018. Climate warming over the past half century has led to thermal degradation of permafrost on the Qinghai-Tibet plateau. The Cryosphere, **12**: 595–608. doi:10.5194/tc-12-595-2018.

Schumm, S.A. 1960. The shape of alluvial channels in relation to sediment type. Geological Survey Professional Paper **352-B**: 17–30.

Schumm, S.A. 1977. The fluvial system. John Wiley & Sons, New York.

Seguin, M.K., and Allard, M. 1984. Le pergélisol et les processus thermokarstiques de la région de la rivière Nastapoca, Nouveau-Québec. Géographie physique et Quaternaire, **38**: 11–25. doi:10.7202/032532ar.

Syvitski, J.P.M. 2002. Sediment discharge variability in arctic rivers: implications for a warmer future. Polar Research, **21**: 323–330. doi:10.1111/j.1751-8369.2002.tb00087.x.

Tananaev, N.I. 2015. Hysteresis effects of suspended sediment transport in relation to geomorphic conditions and dominant sediment sources in medium and large rivers of the Russian Arctic. Hydrology Research, **46**: 232–243. doi:10.2166/nh.2013.199.

Veilleux, S., Bhiry, N., and Decaulne, A., 2020. Talus slope characterization in Tasiapik valley (Subarctic Quebec): evidence of past and present slope processes. Geomorphology, **349**: 106911. doi:10.1016/j.geomorph.2019.106911.

Vonk, J.E., Tank, S.E., Bowden, W.B., Laurion, I., Vincent, W.F. Alekseychik, P., et al. 2015: Reviews and synthesis: effects of permafrost thaw on arctic aquatic ecosystems, Biogeosciences, **12**: 7129–7167. doi:10.5194/bg-12-7129-2015.

Walvoord, M.A., and Kurylyk, B.L. 2016. Hydrologic impacts of thawing permafrost: a review. Vadose Zone Journal, **15**(6): 1–20. doi:10.2136/vzj2016.01.0010. PMID: 29398981.

Williams, G.P. 1989. Sediment concentration versus water discharge during single hydrologic events in rivers. Journal of Hydrology, **111**: 89–106. doi:10.1016/0022-1694(89)90254-0.

Wilson, L. 1973. Variations in mean annual sediment yield as a function of mean annual precipitation. American Journal of Science, **273**: 335–349. doi:10.2475/ajs.273.4.335.